Photoionization of Porphyrins in Mesoporous Siliceous MCM-41, AlMCM-41, and TiMCM-41 Molecular Sieves

Hyung Mi Sung-Suh, Zhaohua Luan, and Larry Kevan*

Department of Chemistry, University of Houston, Houston, Texas 77204-5641

Received: August 26, 1997; In Final Form: October 6, 1997[⊗]

The photoionization of *meso*-tetraphenylporphyrin (H_2TPP) within mesoporous MCM-41 silica tube molecular sieves is studied with visible light irradiation at room temperature and 77 K. Porphyrin π-cation radicals ($H_2TPP^{\bullet+}$) are generated by photoionization within MCM-41 molecular sieves and are characterized by electron spin resonance (ESR) and diffuse reflectance UV−vis spectroscopy. Mesoporous MCM-41 molecular sieves are shown to be effective heterogeneous hosts to accomplish long-lived net photoinduced electron transfer of bulky porphyrin molecules at room temperature. Siliceous MCM-41 molecular sieves with different pore sizes designated as C_n-MCM-41 (C_n is the alkyl chain length of the surfactant used in the synthesis) demonstrate a significant pore size effect on the photoionization efficiency of H_2TPP. The $H_2TPP^{\bullet+}$ photoyield in C_n-MCM-41 measured by ESR increases with increasing C_n and is greatest in C_{16}-MCM-41. A series of titanosilicate TiMCM-41 and aluminosilicate AlMCM-41 molecular sieves were synthesized and change the porphyrin photoionization efficiency in comparison with siliceous MCM-41. The photoionization efficiency increases in the order AlMCM-41 < MCM-41 < TiMCM-41. $H_2TPP^{\bullet+}$ radicals are stable in MCM-41 and TiMCM-41 even at room temperature and decay after 30 min photoirradiation by only 5% after 48 h in TiMCM-41 at room temperature.

Introduction

Photoinduced electron transfer in heterogeneous hosts[1−3] such as organic assemblies of vesicles and micelles[4−6] and porous inorganic solids such as zeolites[7−11] and silica gels (or silica)[12−14] has been extensively studied with a goal to establish artificial photoredox systems for solar energy conversion and storage. For this purpose, porphyrin derivatives[2a,6c−f,15−17] have been used as photosensitive electron donors due to their structural and functional similarities to chlorophylls and their absorption of visible light. The photoionization efficiency is generally limited by back electron transfer, which is a major problem to be solved in most photoredox systems.[1−3] The back-electron-transfer rate is retarded in heterogeneous systems compared to homogeneous solution.[1−5] The photoionization efficiency in organic assemblies is higher than that in homogeneous solution, but the photoinduced radicals are not stable at room temperature. In some cases, the photoyields in organic assemblies are limited by the polarity and solubility of photosensitizers in vesicle and micellar solutions.[1−6]

However, photoionization studies in porous inorganic materials such as zeolites[8−11] and silica gels[13,14] have shown that their cages or pores provide an appropriate microenvironment to retard back electron transfer and increase the lifetime of the photogenerated radical ions. This is associated with steric and electrostatic effects in these inorganic materials. A photosensitizer of proper molecular size compared to the pore sizes of such inorganic materials can be incorporated into the pores, and the photoinduced radical ions can even be stable at room temperature. Zeolites have been extensively studied as microheterogeneous hosts for efficient photoinduced electron transfer.[8−11] Photoinduced electron transfer from $Ru(byp)_3^{2+}$ prepared by intracavity synthesis within the supercages of zeolite Y[9] and zeolite X[10] has been reported. Also, aromatic molecules adsorbed on thermally activated zeolite Y[11a,b] or ZSM-5[11c,d] are readily oxidized to their cation radicals, indicating that the zeolite framework can act as an electron acceptor. The diameter of the supercages of zeolite X and Y is 13 Å, and the cage opening is 8 Å.[7] This cage size is too small for bulky porphyrins such as *meso*-tetraphenylporphyrin (H_2TPP) to fit into, since H_2TPP has a square-planar structure of molecular dimensions 15 × 15 Å.[18]

Photoinduced electron transfer from tetramethylbenzidine,[14a] alkylphenothiazines,[14b] and $Ru(bpy)_3^{2+}$ [14c] in amorphous silica gels with different pore diameters has been studied previously. Those studies showed that the silica gel pore size strongly affects the photoyield and that the silica gel framework may act as an electron acceptor.[14a,b] It was suggested that the lower photoyield in silica gels with larger pore sizes correlates with faster radical decay due to a greater mobility of the photoinduced radicals in larger pores.[14a,b] Fewer silanol groups are adjacent to the photoionizable molecules adsorbed in larger pores due to their larger radius of curvature.[14c] The surface silanol groups (≡Si−OH)[12] of silica gels are the principal sites responsible for the adsorption of organic molecules leading to restricted mobility of the molecules in the pores.[13c,d] In large pore silica gels, the relative distance between the adsorbed molecules or photogenerated radicals and surrounding silanol groups is longer than in smaller pore silica gel because of the different radius of curvature with pore size. Thus, there is greater mobility of photogenerated radicals in larger pore silica gels which decreases the net photoyield.[14]

Silanol groups exist as isolated or as vicinal hydroxyl groups on the silica gel surface and the number of silanols is about 5 OH/nm^2.[12a] The number and nature of silanols depend on the preheating temperature of the silica gels. The number of silanols decreases to about 2.5 OH/nm^2 at 400 °C and to about 1.2 OH/nm^2 at 700 °C by dehydroxylation. The photoyield also depends on the preheating temperature of silica gel.[14c] With increasing preheating temperature to 600 °C, the photoyield gradually decreases because the number of silanols is reduced by dehydroxylation.

[⊗] Abstract published in *Advance ACS Abstracts,* November 15, 1997.

S1089-5647(97)02772-7 CCC: $14.00

Amorphous silica gel has an irregular pore structure with no long-range order and a wide pore size distribution compared to zeolites.[12] Therefore, the recently developed mesoporous M41S molecular sieves[19,20] have been studied here as heterogeneous hosts to accomplish long-lived photoinduced electron transfer of bulky porphyrins. The M41S molecular sieves have been recently synthesized by Mobil scientists.[19] They include MCM-41 with a hexagonal arrangement of tubes, MCM-48 with a cubic structure, and several layered structures. MCM-41 molecular sieves show a regular hexagonal array of uniform silica tubes with diameters from 15 to 100 Å, a high surface area of about 1000 m^2/g, and a pore size distribution nearly as sharp as that of zeolites.[19,20] The MCM-41 materials with these unique properties have promising utility for photoreactions of bulky molecules in addition to catalysis and separation of large organic molecules. The tetrahedral Si^{4+} in the MCM-41 framework can be replaced by other metal ions such as Al^{3+}, Ti^{4+}, Mn^{2+}, and several transition-metal ions.[21−23] This makes it possible to modify the MCM-41 framework to enhance the photoionization efficiency from incorporated molecules such as porphyrins. Only a few studies of photoinduced electron transfer from bulky molecules such as 2,4,6-triphenylpyrylium cation[25a] and tritylium cation[25b] in MCM-41 have been reported.

In this research, a series of mesoporous siliceous C_n-MCM-41 materials with different pore sizes, aluminosilcate AlMCM-41, and titanosilicate TiMCM-41 molecular sieves have been synthesized and used as heterogeneous hosts for long-lived photoinduced electron transfer from bulky *meso*-tetraphenylporphyrin (H_2TPP). The photoionization of H_2TPP in the tubular channels of these mesoporous MCM-41 materials is achieved with visible light ($\lambda > 350$ nm) excitation at room temperature and 77 K, and the photoinduced $H_2TPP^{\bullet+}$ cation is characterized by ESR and diffuse reflectance (DR) UV−vis spectroscopy. The associated photoproduced electron is presumably trapped at a site in the silica framework but is not separately detectable by ESR or DR. It has been found that the $H_2TPP^{\bullet+}$ photoyield in siliceous C_n-MCM-41 samples measured by ESR depends on the pore sizes of C_n-MCM-41. The $H_2TPP^{\bullet+}$ photoyield increases in the order AlMCM-41 < MCM-41 < TiMCM-41, indicating that framework modification by incorporating the Ti^{4+} into the MCM-41 enhances the electron-accepting ability of the MCM-41 framework. $H_2TPP^{\bullet+}$ radicals are stable even at room temperature as well as at 77 K and decay slowly in siliceous MCM-41 and TiMCM-41 compared to AlMCM-41 at room temperature.

Experimental Section

Materials. Sodium silicate solution (27 wt % silica and 14 wt % NaOH, Aldrich) and fumed silica (Sigma) were used as silicon sources. The quaternary ammonium surfactant compounds [$C_nH_{2n+1}(CH_3)_3NBr$ with $n = 10$, 12, 14, and 16] were obtained from TCI America for $n = 10$, 12 and from Aldrich for $n = 14$, 16. The $C_{16}H_{33}(CH_3)_3NOH/Cl$ (CTACl/OH) solution was prepared by batch exchange of a 25 wt % aqueous solution of $C_{16}H_{33}(CH_3)_3NCl$ (Aldrich) using an IRA-420(OH) ion-exchange resin (Aldrich).[19,21] A 25 wt % aqueous solution of tetramethylammonium hydroxide (TMAOH) was obtained from Aldrich. The aluminum source for the AlMCM-41 synthesis was aluminum sulfate obtained from Aldrich, and the titanium source for the TiMCM-41 synthesis was titanium(IV) ethoxide from Aldrich. Anatase TiO_2 with a 50 Å particle diameter was obtained from Sigma. Ammonium titanyl oxalate from Aldrich was used to prepare impregnated TiO_2/MCM-41. Silica gels (powder) with a wide range of pore sizes (17, 22, 25, 40, 60, and 150 Å) were used for a test of pore size effects on the $H_2TPP^{\bullet+}$ photoyield to compare with siliceous C_n-MCM-41. The 17 Å pore silica gel was prepared using sol−gel synthesis by Xiang.[14b] Silica gels with 22 and 25 Å pores were obtained from Sigma, and the others were from Aldrich. The BET surface areas of the silica gels of 17, 22, 25, 40, 60, and 150 Å pore diameters are 600, 560, 505, 750, 480, and 300 m^2/g, respectively. *meso*-Tetraphenylporphyrin designated as H_2TPP was obtained from Aldrich.

MCM-41 Synthesis. *Siliceous C_n-MCM-41.* Siliceous C_n-MCM-41 molecular sieves with different pore sizes were synthesized from sodium silicate and $C_nH_{2n+1}(CH_3)_3NBr$ ($n =$ 10, 12, 14, and 16) surfactants according to Beck et al.[19c] Each $C_nH_{2n+1}(CH_3)_3NBr$ surfactant (0.046 mol) was dissolved in 88−100 g of water to make an 11 wt % solution, and 20.4 g of sodium silicate was added slowly with stirring. This silicate−surfactant mixture was stirred for 30 min, and then the pH was adjusted to 10 by adding dilute sulfuric acid slowly with stirring. The molar composition of the final gel mixture was 1 SiO_2: 0.50 surfactant:0.39 Na_2O:60 H_2O. The resultant gels were crystallized in Teflon-lined autoclaves at 150 °C for 6 days. After cooling to room temperature, the solid products were centrifuged, filtered, washed with distilled water, and dried in air at 100 °C. The products were then calcined at 550 °C for 24 h in flowing air.

AlMCM-41. The synthetic procedure[21a] for AlMCM-41 was as follows. Tetramethylammonium hydroxide (TMAOH) solution (10 g) was combined with 5.9 g of sodium silicate dispersed in 50 g of water with stirring, and then 34.3 g of CTACl/OH solution and 4.52 g of silica were added and stirred for 2 h. The required amount of $Al_2(SO_4)_3$ was dissolved in water and slowly added to the gel. The pH was adjusted to 11 by adding dilute sulfuric acid slowly. The molar composition of the final gel mixture was 1 SiO_2:0.27 CTACl/OH:0.13 Na_2O:0.26 TMAOH:60 H_2O:(0.017−0.033) Al_2O_3. The resultant gels were treated as described above. These samples are designated as AlMCM-41-(*x*), where *x* is the Si/Al ratio in the gel.

TiMCM-41. Titanosilicate TiMCM-41 was synthesized[21b] by the same procedure used for AlMCM-41 except that a titanium source was added instead of an aluminum source. The required amount of titanium(IV) ethoxide was dissolved in a mixture of water and hydrogen peroxide and then added slowly into the silicate−CTACl/OH gel. The pH was then adjusted to 11 with dilute sulfuric acid. The molar composition of the final gel mixture was 1 SiO_2:0.27 CTACl/OH:0.13 Na_2O:0.26 TMAOH: 60 H_2O:(0.013−0.05) TiO_2. The resultant gels were crystallized as described above. These samples are designated as TiMCM-41-(*x*), where *x* is the Si/Ti ratio in the gel. For comparison, impregnated TiO_2−MCM-41 (Si/Ti = 20) was prepared by incipient-wetness impregnation[38] using 0.5 g of siliceous C_{16}-MCM-41 and 3 mL of an aqueous solution containing 0.12 g of ammonium titanyl oxalate. This slurry was stirred for 24 h, dried, and then calcined at 550 °C in flowing air for 24 h.

Characterization. X-ray powder diffraction (XRD) patterns of all MCM-41 samples were recorded on a Philips 1840 powder diffractometer using Cu Kα radiation of wavelength 1.541 Å, a 0.0025° step size, and 1 s step time over the range $1.5° < 2\theta < 15°$. The specific surface areas (*S*) of all MCM-41 and silica gel samples were measured by the BET (Brunauer−Emmett−Teller) method with N_2 physisorption at 77 K using a Quantachrome Monosorb analyzer. The diffuse reflectance (DR) UV−vis spectra were recorded using a Perkin-Elmer Model 330 spectrometer with an integrating sphere accessory.

Samples for Photoionization. All MCM-41 materials and silica gels were dried at 200 °C for 24 h to remove the physisorbed water before introducing H_2TPP. To adsorb H_2-

TABLE 1: Structural Properties of Siliceous C_n-MCM-41, TiMCM-41, and AlMCM-41

sample	d_{100} (Å)	a_0[a] (Å)	pore size[b] (Å)	BET surface area (m^2/g)
C_{10}-MCM-41	27.1	31.3	21	1030
C_{12}-MCM-41	29.3	33.8	24	1160
C_{14}-MCM-41	33.5	38.7	29	1230
C_{16}-MCM-41	37.1	42.7	33	1280
TiMCM-41				
Si/Ti = 80	37.6	43.4	33	953
Si/Ti = 40	36.7	42.4	32	970
Si/Ti = 20	36.2	41.8	32	920
Si/Ti = 10	34.9	40.3	30	780
AlMCM-41				
Si/Al = 60	36.2	41.8	32	940
Si/Al = 30	36.3	41.9	32	905

[a] $a_0 = 2d_{100}/\sqrt{3}$. [b] Pore sizes are obtained by subtracting 10 Å from the a_0 values assuming the pore wall thickness is ~10 Å.[20]

TPP into silica gel, C_n-MCM-41, AlMCM-41, and TiMCM-41, 2 mL (0.3−1.6 g) of each MCM-41 or silica gel sample was immersed into 3 mL of chloroform containing a suitable amount (1.1−6.0 μmol) of H_2TPP which depends on the surface areas of the MCM-41 and silica gel samples. This slurry of MCM-41 or silica gel powder in H_2TPP solution was stirred and allowed to equilibrate for 24 h, and the solvent was then removed under vacuum.[31,32a] For 17, 22, 25, 40, 60, and 150 Å pore silica gels, the loading amounts of H_2TPP were 3.8, 4.2, 3.7, 4.7, 3.0, and 1.8 μmol/g of silica gel, respectively. For siliceous C_n-MCM-41 samples, the loadings of H_2TPP were 6.1 μmol/g of C_{10}-MCM-41, 6.9 μmol/g of C_{12}-MCM-41, 7.3 μmol/g of C_{14}-MCM-41, and 7.6 μmol/g of C_{16}-MCM-41. For H_2TPP/AlMCM-41 samples, the loadings of H_2TPP were 5.6 μmol/g of AlMCM-41-(30) and 5.3 μmol/g of AlMCM-41-(60). For H_2TPP/TiMCM-41 samples, the loadings of H_2TPP were 4.6 μmol/g of TiMCM-41-(10), 5.4 μmol/g of TIMCM-41-(20), 5.7 μmol/g of TiMCM-41-(40), and 5.7 μmol/g of TiMCM-41-(80). In each H_2TPP/MCM-41 or silica gel sample, the loading amounts of H_2TPP shown above correspond to about 2.3% coverage (or 0.017 μmol/m^2) of the surface area for each MCM-41 or silica gel as follows. Assuming a uniform distribution of H_2TPP, the contact area of each H_2TPP molecule is about 2.25 nm^2 calculated from the dimensions of a square-planar H_2TPP molecule (1.5 × 1.5 nm).[18] The surface coverage by H_2TPP in each MCM-41 or silica gel sample is estimated from the amount of H_2TPP loading and the surface area of each support in Table 1. With the low loading amounts of H_2TPP in the MCM-41 and silica gel samples, each H_2TPP molecule occupies a relatively large surface area of 100 nm^2. It is assumed that the H_2TPP molecules are dispersed uniformly and that intermolecular interaction between two neighboring H_2TPP molecules is improbable.

These low loadings for porphyrins correspond to optimal photoyields. If the loadings are increased, the percent photoyields decrease, presumably because of less efficient electron transfer to the silica surface which acts as an electron acceptor.

The same amount of each dried H_2TPP/MCM-41 sample was transferred into a Suprasil quartz tube (2 mm i.d. × 3 mm o.d.) which was sealed at one end. The sample tube was evacuated to about 10^{-4} Torr for 24 h and was flame-sealed. All samples were prepared in the dark.

Photoirradiation and Radical Analysis. The evacuated H_2TPP/MCM-41 samples were irradiated with a 300 W Cermax xenon lamp (ILC-LX 300 UV) at room temperature or at 77 K. The light was passed through a 10 cm water filter and a Corning No. 0-51 glass filter which passes light of wavelength longer than 350 nm. Each sample was irradiated in a quartz dewar that was rotated at 4 rpm to ensure even irradiation of the samples. The photoinduced $H_2TPP^{\bullet+}$ was identified by ESR and diffuse reflectance (DR) UV−vis spectroscopy. No associated photoproduced electron center is observed by ESR or DR; it could be hidden under the ESR spectra of H_2TPP^+ and the DR spectra of H_2TPP^+ and H_2TPP. The ESR spectra were recorded at X-band using a Bruker ESP 300 spectrometer with 100 kHz magnetic field modulation. The microwave power was 0.2 mW at room temperature and 0.02 mW at 77 K to avoid power saturation. The photoinduced $H_2TPP^{\bullet+}$ yields were determined by double integration of the ESR spectra using the ESP 300 software and were calibrated by a 1,1′-diphenyl-2-picrylhydrazyl (DPPH) standard. Each photoyield is an average of three determinations. The H_2TPP/MCM-41 samples were evacuated in an cylindrical quartz optical cell at 10^{-4} Torr for 24 h, and then the DR UV−vis spectra of the H_2TPP/MCM-41 samples were recorded before and after 30 min photoirradiation at room temperature. Thirty minutes was selected for photoirradiation because the photoyield reaches a plateau after this time.

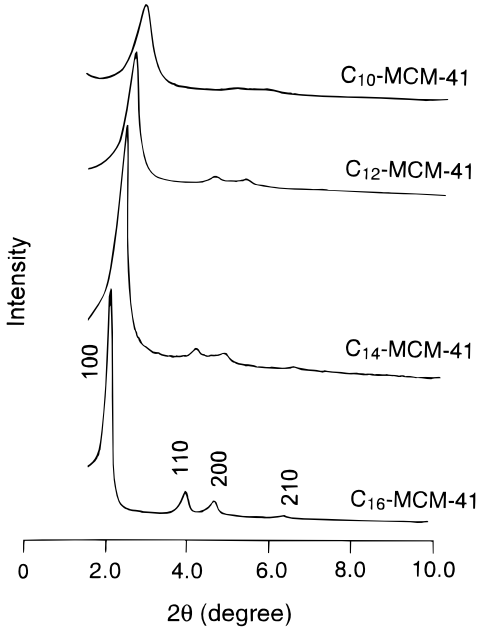

Figure 1. XRD patterns of calcined C_n-MCM-41.

Results

MCM-41 Samples. The XRD patterns of siliceous C_n-MCM-41 molecular sieves with different pore sizes are shown in Figure 1. The XRD patterns of the MCM-41 samples are indexed on a hexagonal lattice as assigned previously.[19] The hexagonal unit cell parameter (a_0) is calculated as $2d_{100}/\sqrt{3}$ from d_{100} which is obtained from 2θ of the first peak in the XRD pattern by Bragg's equation[26] ($2d \sin\theta = \lambda$, $\lambda = 1.5417$ Å for the Cu Kα line). The value of a_0 is equal to the internal pore diameter plus one pore wall thickness. Table 1 shows the BET surface areas, the hexagonal unit cell parameters (a_0), and the pore sizes of siliceous C_n-MCM-41, TiMCM-41, and AlMCM-41. The pore sizes of the MCM-41 samples were calculated by subtracting an estimated 10 Å thickness for the pore wall[20,27] from the value of a_0. Stucky et al. have reported that theoretical calculation using a hexagonal model of cylindrical pores for MCM-41 gives a pore wall thickness of 8 ± 1 Å.[20] A variety of other MCM-41 pore wall thicknesses have been reported.[19b,23a,27,28] From a comparative study of MCM-41 pore sizes, it has been shown that the conventional BJH analysis of adsorption isotherm data gives pore wall thicknesses of MCM-

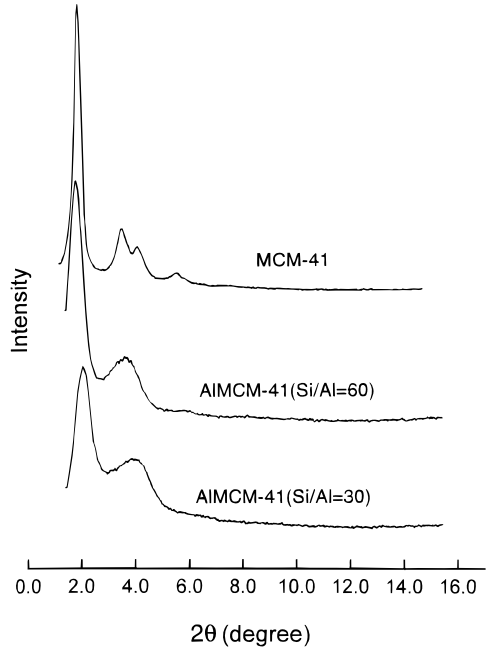

Figure 2. XRD patterns of calcined AlMCM-41.

41 of 15−16 Å, and a calculation by nonlocal density functional theory gives wall thicknesses of 4−5.5 Å.[27,28] Thus, an average of 10 Å seems reasonable to use.

C_n-MCM-41. As the alkyl chain length of the surfactants in the syntheses of C_n-MCM-41 increases, the first XRD peaks (d_{100}) move to lower 2θ and the values of the hexagonal unit cell parameter (a_0) increase, which indicates that the pore sizes of C_n-MCM-41 depend on C_n. C_{12}-MCM-41, C_{14}-MCM-41, and C_{16}-MCM-41 exhibit-well resolved XRD patterns in the 2°−7° range of 2θ typical of hexagonal MCM-41 as described by Beck et al.[19] The XRD pattern of C_{10}-MCM-41 shows less well-resolved peaks in the 2°−7° range of 2θ in comparison with other C_n-MCM-41 samples. But C_{10}-MCM-41 still clearly has a hexagonal mesoporous phase.[19b,c]

AlMCM-41-(x). The XRD patterns of AlMCM-41-(30) and AlMCM-41-(60) are shown in Figure 2. Compared to siliceous MCM-41, the XRD peaks of AlMCM-41 are broader and less resolved and the intensity of the first peak decreases as the Al content increases. The BET surface areas of the AlMCM-41 samples are lower than that of siliceous C_{16}-MCM-41.

TiMCM-41-(x). For TiMCM-41 (Si/Ti = 10, 20, 40, and 80) the resolution and intensity of the XRD peaks decreases as the Ti content increases as shown in Figure 3. TiMCM-41-(10) gives the least well-defined XRD pattern and a lower surface area in comparison with the other TiMCM-41 samples as shown in Table 1. The DR UV−vis spectra of the TiMCM-41 samples are shown in Figure 4. Compared to bulk anatase (TiO_2 particles of 50 Å diameter), the absorption edges of all TiMCM-41 samples are blue-shifted by more than 50 nm. The TiMCM-41 samples of low Ti content (Si/Ti ≥ 20) show absorption bands centered at 220−230 nm which can be assigned to ligand-to-metal charge-transfer transitions between the oxygen ligands to tetracoordinated Ti^{4+} ions.[23,24] This indicates that the Ti^{4+} ions are incorporated into the framework of MCM-41.[21b,23] The DR UV−vis spectra of the TiMCM-41 samples show no significant absorption at 300−350 nm, which indicates that a segregated crystalline TiO_2 phase like anatase is absent in TiMCM-41. But, TiMCM-41-(10) of higher Ti content shows a broad, red-shifted absorption band at 200−350 nm compared to TiMCM-41 with lower Ti contents. This indicates that the Ti^{4+} ions in TiMCM-41-(10) are present partly in tetrahedral

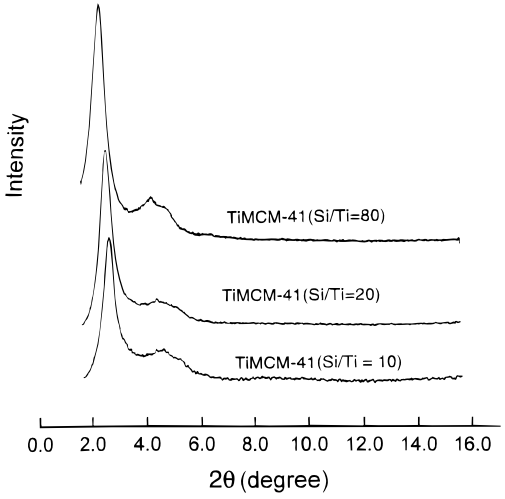

Figure 3. XRD patterns of calcined TiMCM-41.

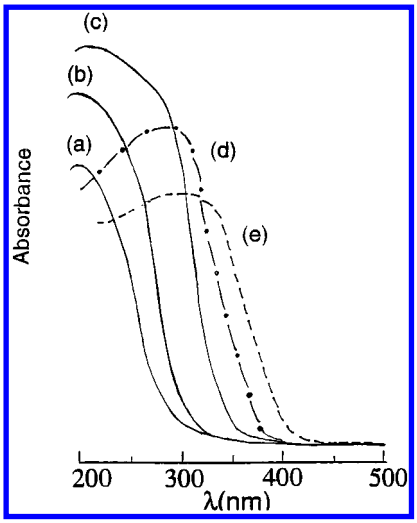

Figure 4. Diffuse reflectance UV−vis spectra of (a) TiMCM-41-(80), (b) TiMCM-41-(20), (c) TiMCM-41-(10), (d) impregnated TiO_2−MCM-41 (Si/Ti = 20), and (e) anatase with 50 Å particle diameter.

coordination in the framework and partly as TiO_2 particles. Also, TiMCM-41-(10) shows a poorly resolved XRD pattern, a lower surface area, and a decrease in the unit cell parameter (pore size) as shown in Figure 3 and Table 1. This probably arises from a partial loss of structure for high Ti incorporation.[23] These results are consistent with previous characterization results[21b,23] of TiMCM-41 samples with different Ti contents, although the interpretation of the characterization data of the Ti species in the TiMCM-41 is still under debate.[24a]

$H_2TPP^{\bullet+}$ Analysis by ESR and DR UV−vis Spectroscopy. The ESR spectra from photoinduced $H_2TPP^{\bullet+}$ in MCM-41 after 30 min photoirradiation with $\lambda > 350$ nm at room temperature and 77 K are shown in Figure 5. The ESR signal obtained from each photoirradiated H_2TPP/MCM-41 material shows a singlet at $g = 2.0028$ with a line width of 6 G which is assigned to $H_2TPP^{\bullet+}$.[15b,32] The silica gel and MCM-41 samples without H_2TPP give no ESR signals after photoirradiation. The DR UV−vis spectra of H_2TPP/MCM-41, AlMCM-41, and TiMCM-41 are shown before and after photoirradiation at room temperature in Figure 6. After photoirradiation, a new absorption band appears in the 700−800 nm range. This is assigned to photogenerated $H_2TPP^{\bullet+}$.[16,32a]

Photoyield in C_n-MCM-41 versus Silica Gels of Different Pore Diameters. To investigate the $H_2TPP^{\bullet+}$ photoyield over a wider range of pore diameters, the photoionization of H_2TPP in a series of silica gels with pore diameters of 17−150 Å has

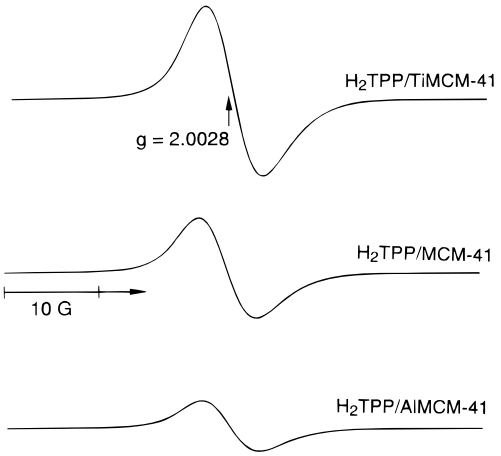

Figure 5. ESR spectra of photoinduced $H_2TPP^{\bullet+}$ in TiMCM-41, MCM-41, and AlMCM-41 after 30 min irradiation with $\lambda > 350$ nm at room temperature.

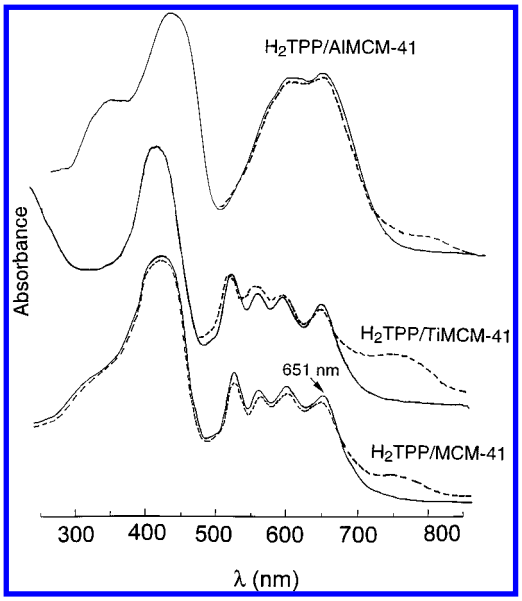

Figure 6. Diffuse reflectance UV−vis spectra of H_2TPP in MCM-41, TiMCM-41, and AlMCM-41 before (—) and after (···) 30 min irradiation with $\lambda > 350$ nm at room temperature.

been studied, and the $H_2TPP^{\bullet+}$ photoyields are shown in Figure 7a. The $H_2TPP^{\bullet+}$ photoyield depends on the pore diameter of the silica gel, is largest in the 40 Å pore silica gel, and decreases in silica gels with larger pores (60 and 150 Å). H_2TPP/17 Å pore silica gel shows no $H_2TPP^{\bullet+}$ photoyield. For H_2TPP/C_n-MCM-41 samples, the $H_2TPP^{\bullet+}$ photoyields also depend on the pore sizes of C_n-MCM-41 as shown in Figure 7b. The $H_2TPP^{\bullet+}$ photoyield is largest in C_{16}-MCM-41 (33 Å pore size) and smallest in C_{10}-MCM-41 (21 Å pore size). The color of evacuated H_2TPP/C_n-MCM-41 is dark brown, which turns to green after photoirradiation. C_{16}-MCM-41 will be designated simply as MCM-41 from now on. The photoyield at 77 K is higher than that at room temperature as shown in Figure 8. H_2-$TPP^{\bullet+}$ radicals do not decay at 77 K and are relatively stable even at room temperature. At room temperature after 30 min photoirradiation, $H_2TPP^{\bullet+}$ radicals decay by 10% after 48 h and by 40% after 240 h based on the decrease in ESR intensity.

Photoyield in AlMCM-41. H_2TPP/AlMCM-41 samples give lower $H_2TPP^{\bullet+}$ photoyields in comparison with TiMCM-41 and MCM-41 as shown in Figure 8. The photoyield decreases with increasing Al content in AlMCM-41 as shown in Figure 9. As shown in Figure 10a,b, the UV−vis absorption spectrum of the H_2TPP solution after contact with AlMCM-41 for impregnation

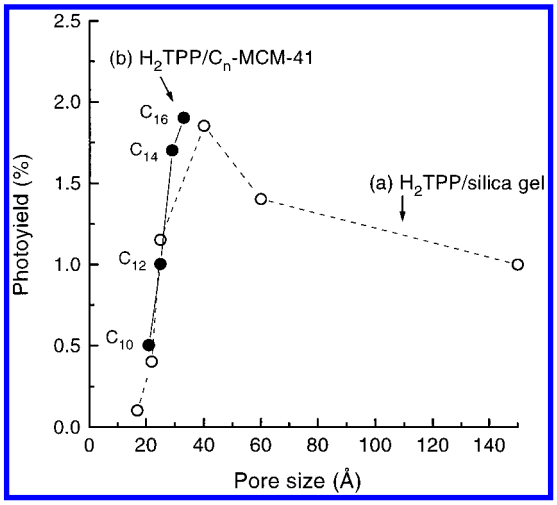

Figure 7. $H_2TPP^{\bullet+}$ photoyields in (a) silica gels and (b) siliceous C_n-MCM-41 molecular sieves with different pore sizes after 30 min irradiation with $\lambda > 350$ nm at room temperature.

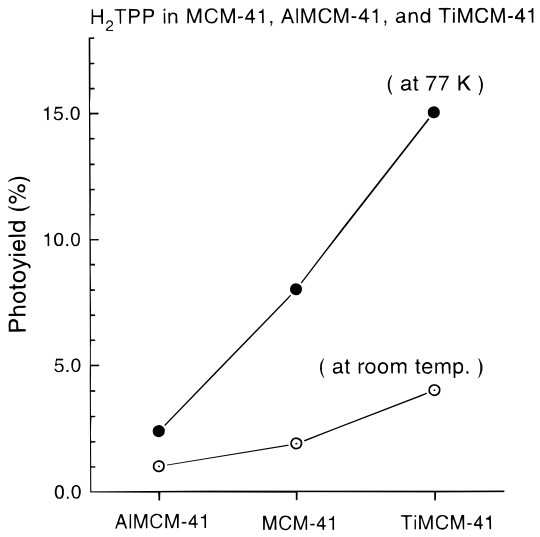

Figure 8. $H_2TPP^{\bullet+}$ photoyields in siliceous MCM-41, TiMCM-41-(20), and AlMCM-41-(30) after 30 min irradiation with $\lambda > 350$ nm at room temperature and 77 K.

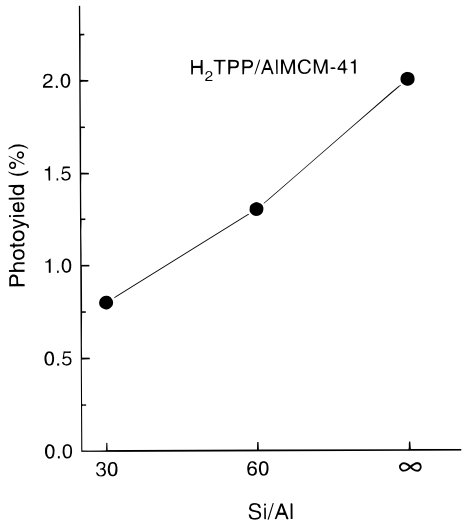

Figure 9. $H_2TPP^{\bullet+}$ photoyields in AlMCM-41 samples versus Al content after 30 min irradiation with $\lambda > 350$ nm at room temperature.

is different from that before contact with AlMCM-41. The Q-bands are red-shifted and the relative absorbances change. The DR UV−vis spectra of H_2TPP/AlMCM-41 are different

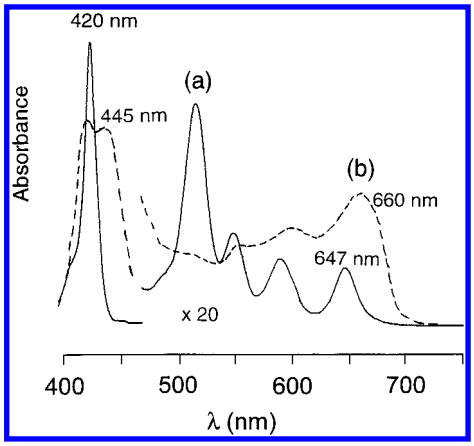

Figure 10. UV−vis absorption spectra of H_2TPP in chloroform solution (a) before and (b) after contact with AlMCM-41.

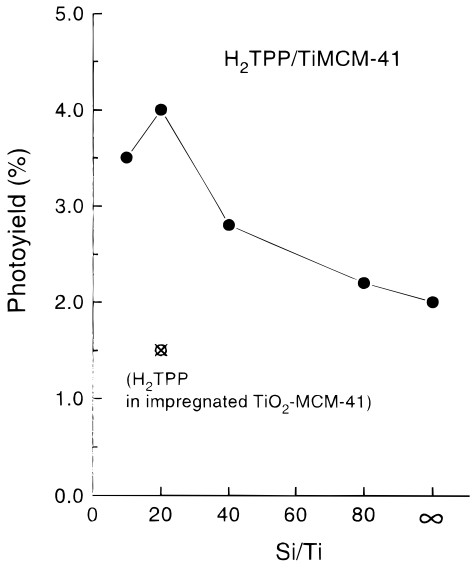

Figure 11. $H_2TPP^{\bullet+}$ photoyields in TiMCM-41 versus Ti content after 30 min irradiation with $\lambda > 350$ nm at room temperature.

from those of H_2TPP/MCM-41 and TiMCM-41 as shown in Figure 6. The color of the H_2TPP solution changes from purple to green after contact with AlMCM-41, and the color of an evacuated powder sample of H_2TPP/AlMCM-41 is bluish green. This color change does not happen in H_2TPP/MCM-41 and H_2-TPP/TiMCM-41. At room temperature, $H_2TPP^{\bullet+}$ radicals in AlMCM-41 decay after photoirradiation by 40% after 48 h, which is faster than in siliceous MCM-41.

Photoyield in TiMCM-41. Figure 11 shows that the H_2-$TPP^{\bullet+}$ photoyield is greatest in TiMCM-41 in comparison with siliceous MCM-41 and AlMCM-41. The photoyield in TiMCM-41 increases with increasing Ti content in TiMCM-41 as shown in Figure 11. The photoyield increases to a Si/Ti ratio of 20 and then decreases for a Si/Ti ratio of 10. The color of fresh evacuated H_2TPP/TiMCM-41 is dark brown and turns to green after photoirradiation, which is the same as for H_2TPP/MCM-41. After photoirradiation, the absorbance at 700−800 nm in the DR UV−vis spectrum of H_2TPP/TiMCM-41 increases more in comparison with photoirradiated H_2TPP/MCM-41 and H_2-TPP/AlMCM-41 as shown in Figure 6. Also, the $H_2TPP^{\bullet+}$ photoyield is larger at 77 K than at room temperature as shown in Figure 8. $H_2TPP^{\bullet+}$ radicals do not decay at 77 K and decay after photoirradiation by only 5% after 48 h at room temperature. The enhancement of the photoyield in TiMCM-41 is discussed below.

Discussion

The ESR signal of $H_2TPP^{\bullet+}$ in Figure 5 shows a singlet with $g = 2.0028$, which is consistent with the g values of porphyrin cation derivatives.[15b,32] The ESR signal of $H_2TPP^{\bullet+}$ in each MCM-41 sample has a line width of 5.5 G at room temperature and 6.5 G at 77 K. The small increase in the line width of the ESR signal at 77 K results from a mobility decrease of H_2-$TPP^{\bullet+}$ inside the MCM-41 pores as reported previously for phenothiazine cation radical in silica gels.[14b] It has been found that the $H_2TPP^{\bullet+}$ photoyield in MCM-41 is higher at 77 K than at room temperature. This can be explained, as for the phenothiazine/silica gel system, by the porphyrin cation mobility decreasing at 77 K which reduces the probability of back electron transfer from the silica gel framework to the phenothiazine cation and so decreases the photoyield.[14b] The photoionization of porphyrins is usually a two-photon process via the triplet state, and the triplet lifetime (τ_p) and quantum yield are longer at lower temperature.[29,30] For triplet H_2TPP, τ_p is 6 ms at 77 K and 1.4 ms at room temperature.[30b] The increase in the triplet quantum yield and lifetime at 77 K results in a higher $H_2TPP^{\bullet+}$ photoyield at 77 K than at room temperature.

UV−vis Spectra. Figure 10a shows an absorption spectrum of H_2TPP in chloroform. This spectrum consists of the Soret band (420 nm) and four Q-bands (515, 550, 615, 646 nm). The absorbance of the Soret band is about 20 times higher than that of the Q-bands.[16a,32c] In Figure 6 of the DR UV−vis spectra of powder samples of H_2TPP/MCM-41, the Soret band becomes broader, and the absorbance of the Soret band of H_2TPP decreases in comparison with the H_2TPP spectra in solution in Figure 10a. The absorbance of the Soret band of H_2TPP/MCM-41 is only 2 times greater than that of the Q-bands. The Q-band at 650 nm for H_2TPP in MCM-41 and TiMCM-41 is red-shifted by 3 nm compared to the Q-band at 647 nm in Figure 10a of H_2TPP in chloroform. It has been shown that adsorption of organic molecules on oxide supports produces strong perturbations of the absorption maxima and the molar absorption coefficients.[31] The electronic spectroscopy and the surface photochemistry of organic molecules adsorbed on silica gel have been studied.[13c,d,31,32a] The results have shown that adsorption generally produces spectral red shifts if the excited state of the molecule has an increased permanent dipole or if it is more polarizable than the ground state and spectral blue shifts if the reverse is true. The broadening of electronic absorption bands of aromatic molecules adsorbed on silica gels is attributed to π-electron interaction with surface hydroxyl groups.[31] So, a slight red shift of the Q-bands and a large absorbance decrease and broadening of the Soret band in Figure 6 for H_2TPP in MCM-41 indicate that H_2TPP molecules are adsorbed onto MCM-41 and that the porphyrin π-electrons interact with the surface hydroxyl groups of MCM-41. Similar spectral changes for porphyrin adsorption on oxide surfaces have been reported for ZnTPP on TiO_2[17d] and for CoTPP and H_2TPP on TiO_2 and silica gel.[32a]

As shown in Figure 6, a new broad absorption band appears at 700−800 nm for H_2TPP/MCM-41 after photoirradiation which is assigned to $H_2TPP^{\bullet+}$.[16] So, the absorbance increase at 700−800 nm is proportional to the $H_2TPP^{\bullet+}$ photoyield in MCM-41.

Photoionization in C_n-MCM-41. *Pore Size Effect.* The change of the $H_2TPP^{\bullet+}$ photoyield with the alkyl chain length (C_n) of the surfactant used in the synthesis is attributed to the different pore diameters of the C_n-MCM-41 samples. The photoionization of H_2TPP in silica gels with a broader range of pore diameters (17−150 Å) shown in Figure 7a supports the C_n-MCM-41 pore size effect on the $H_2TPP^{\bullet+}$ photoyield. The

$H_2TPP^{\bullet+}$ photoyield is largest in the 40 Å pore silica gel and decreases in the silica gels of larger pore diameters. The lower photoyields in silica gels of larger pore sizes correlate with faster radical decay due to greater mobility of the photoinduced radicals in larger pores[14b] and with fewer adjacent silanol groups due to the larger radius of curvature in larger pores.[14c] H_2TPP is adsorbed on silica gel via a π-electron interaction with the surface silanol groups.[13c,d,31] H_2TPP trapped in 40 Å pore silica gel is surrounded by several adjacent silanols. But, in 150 Å pore silica gel, there are fewer adjacent silanols to H_2TPP because of its smaller radius of curvature.[14c] So, the overall interaction between H_2TPP and surface silanol groups is weaker in larger pores, resulting in greater mobility of H_2TPP or $H_2TPP^{\bullet+}$ and a lower net photoyield.

When H_2TPP is adsorbed on silica gel or MCM-41 from chloroform solution, the pore structure is covered by an adsorbed chloroform layer. H_2TPP then interacts with the chloroform layer adsorbed on the internal surface of a pore.[31b] Thus, the effective pore diameter of silica gel or MCM-41 is decreased by the thickness of the adsorbed chloroform layer during impregnation with H_2TPP in chloroform. The kinetic diameter of chloroform ($CHCl_3$) is about 4 Å calculated from the bond lengths (C—H, 1.1 Å, C—Cl, 1.76 Å), the 109° bond angle, and the radii of H (1.2 Å) and Cl (1.8 Å).[33] If the pore structure is assumed to be cylindrical, the pore diameter of silica gel or MCM-41 is decreased by about 8 Å due to the chloroform layer adsorbed on the internal surface of the pores. To then adsorb H_2TPP inside a pore, the pore diameter must be larger than 23 Å. This explains the low photoyields in 17 and 22 Å pore silica gels.

The 21 Å pore of C_{10}-MCM-41 is not large enough to contain H_2TPP, which gives a lower H_2TPP photoyield than in other C_n-MCM-41 samples. C_{16}-MCM-41 seems to have the optimum pore size (~33 Å) for containing H_2TPP and stabilizing the photoinduced porphyrin radical cation within the pores.

In previous studies[6d−f] of the photoionization of alkylporphyrins in vesicle solutions such as dipalmitoylphosphatidylcholine, dioctadecyldimethylammonium chloride, and hexadecyl phosphate, the porphyrin cation radicals are not stabilized at room temperature. The solubilization limit of alkylporphyrins into these vesicle solutions is about 0.4 μmol of alkylporphyrin per 1 mL of vesicle solution. A porphyrin with no pendent alkyl chain like H_2TPP is not solubilized into such vesicle solutions.[6f] The photoyield of photogenerated porphyrin cation radicals is limited by the solubility of the porphyrins in such vesicle solutions. But, in mesoporous MCM-41 molecular sieves, adsorbed porphyrins with or without pendent alkyl chains form stable photoinduced porphyrin cation radicals at room temperature as well as at 77 K. So, mesoporous MCM-41 materials are promising hosts to achieve long-lived photoinduced charge separation of porphyrins at room temperature.

Photoionization in AlMCM-41. The $H_2TPP^{\bullet+}$ photoyield increases in the order AlMCM-41 < MCM-41 < TiMCM-41 as shown in Figure 8. The absorption spectrum of the H_2TPP solution after contact with AlMCM-41 in Figure 10b looks like the spectrum of H_2TPP mixed with diprotonated H_2TPP (H_4TPP^{2+}).[16,32c] As shown in Figure 10b, the Soret band splits into two bands which consist of a 420 nm band from H_2TPP and a new band at 445 nm from H_4TPP^{2+}, and the Q-band at 660 nm is also red-shifted compared to the Q-band at 650 nm of H_2TPP in Figure 10a.[32c] The DR UV−vis spectrum of evacuated H_2TPP/AlMCM-41 powder also shows a similar spectral change in comparison with those of H_2TPP/MCM-41 and TiMCM-41 in Figure 6. The color of the H_2TPP solution after contact with AlMCM-41 changes from purple to green. These changes in color and spectrum of H_2TPP in AlMCM-41 are enhanced as the Al content in AlMCM-41 increases, indicating that H_2TPP is protonated during contact with the acidic surface of AlMCM-41.[34a] So, the lower $H_2TPP^{\bullet+}$ photoyield in AlMCM-41 compared to siliceous MCM-41 seems to result from the protonation of H_2TPP on acidic AlMCM-41. It has been shown that H_4TPP^{2+} gives strong fluorescence and weak phosphorescence[16c] and that the weak phosphorescence results from a lower triplet yield. Porphyrin photoionization generally occurs via the triplet state.[29,30] So, the lower $H_2TPP^{\bullet+}$ photoyield in AlMCM-41 compared to siliceous MCM-41 seems to result from protonation of H_2TPP on AlMCM-41 because the protonated H_2TPP (H_4TPP^{2+}) has a lower triplet yield than H_2TPP.[16c] The faster decay of $H_2TPP^{\bullet+}$ in AlMCM-41 compared to siliceous MCM-41 is also due to protonation of the photoinduced porphyrin radicals on the acidic surface of AlMCM-41.

Photoionization in TiMCM-41. H_2TPP/TiMCM-41 shows a higher photoyield than pure siliceous MCM-41. The photoyield increases as the Ti content increases to a Si/Ti ratio of 20 as shown in Figure 11. A decrease in the $H_2TPP^{\bullet+}$ photoyield in TiMCM41 for a Si/Ti ratio of 10 may result from a lower surface area and smaller pore size of TiMCM-41-(10) as shown in Figure 3 and Table 1, probably due to structural imperfection from high Ti incorporation.[23] For H_2TPP/ impregnated TiO_2−MCM-41 (Si/Ti = 20), there is no photoyield enhancement due to titanium addition, and the photoyield is even lower than in siliceous MCM-41 as shown in Figure 11. The TiO_2 particle size in impregnated TiO_2−MCM-41 sample is estimated as about 36 Å from the absorption edge (375 nm) position of impregnated TiO_2−MCM-41 compared with that (400 nm) of 50 Å TiO_2 (anatase) particles in Figure 4, using a formula for the particle size dependence of the semiconductor bandgap energy given by Brus[35a,b] and modified by Wang et al.[35c] So, the TiO_2 particles in impregnated TiO_2−MCM-41 seem to be too big to be dispersed inside the 33 Å MCM-41 pores, and most of the TiO_2 particles are probably located outside the MCM-41 pores or block the pores to result in a lower $H_2TPP^{\bullet+}$ photoyield compared to that of siliceous MCM-41.

From the higher $H_2TPP^{\bullet+}$ photoyield and slower radical decay in TiMCM-41 compared to siliceous MCM-41, it is suggested that TiMCM-41 is a better electron acceptor than MCM-41 presumably due to reduction of Ti(IV) in the framework. It has been shown that, for catalytic oxidation reactions of some aromatics, alkenes, and alcohols in titanium-substituted molecular sieves such as TS-1,[24,37] these molecules are selectively adsorbed on Ti(IV) sites.[40] Previously, it has been shown that surface Ti(IV) centers in TiMCM-41 immobilize vanadium species and promote oxidation of VO^{2+} to V^{5+} probably due to the reducibility of Ti^{4+} to Ti^{3+} in TiMCM-41.[38] Similarly, for photoionization of H_2TPP in TiMCM-41, it seems that H_2TPP molecules are preferentially adsorbed at surface Ti(IV) sites, resulting in a higher $H_2TPP^{\bullet+}$ photoyield and slower radical decay compared to siliceous MCM-41. So, it is suggested that the Ti(IV) sites in TiMCM-41 act as electron acceptor sites in contrast to Si(IV).[24,36,39] One may expect to see an ESR signal of Ti^{3+} species[39] generated by photoelectron transfer from H_2TPP, but this is not detected at 77 K possibly due to overlap with the $H_2TPP^{\bullet+}$ ESR signal. Overall, it seems that Ti(IV) in TiMCM-41 modifies the framework to enhance H_2TPP adsorption as well as act as a better electron acceptor site to enhance the $H_2TPP^{\bullet+}$ photoyield and to decrease the radical decay rate.

Conclusions

Mesoporous MCM-41 molecular sieves are found to be promising hosts for long-lived photoinduced charge separation of adsorbed *meso*-tetraphenylporphyrin (H_2TPP). The $H_2TPP^{\bullet+}$ photoyields in siliceous C_n-MCM-41 (C_n = C_{10}, C_{12}, C_{14}, and C_{16}) increase with pore size and are largest in C_{16}-MCM-41 (33 Å pore size). This is supported by H_2TPP photoionization results in silica gels with a wider range of pore sizes (17−150 Å), which show the largest $H_2TPP^{\bullet+}$ photoyield in 40 Å pore silica gel.

The $H_2TPP^{\bullet+}$ photoyield increases in the order AlMCM-41 < MCM-41 < TiMCM-41. Protonation of H_2TPP to H_4TPP^{2+} occurs in AlMCM-41 and results in a lower $H_2TPP^{\bullet+}$ photoyield and faster radical decay compared to those of siliceous MCM-41. For H_2TPP/TiMCM-41, the $H_2TPP^{\bullet+}$ photoyield is higher and the radicals decay more slowly than in siliceous MCM-41. It seems that the Ti(IV) sites in the TiMCM-41 framework enhance the electron-accepting ability of the framework probably by reduction of Ti(IV) in contrast to Si(IV). The photoyield is higher at 77 K than at room temperature. The H_2TPP^{+} radicals do not decay at 77 K and are relatively stable even at room temperature.

Acknowledgment. This research was supported by the Division of Chemical Sciences, Office of Basic Energy Science, Office of Energy Research, U.S. Department of Energy, and by the University of Houston Energy Lab.

References and Notes

(1) Kalyanasundaram, K. *Photochemistry in Microheterogeneous Systems*; Academic: New York, 1987.

(2) (a) *Energy Resources through Photochemistry and Catalysis*; Grätzel, M., Ed.; Academic: New York, 1983. (b) Grätzel, M. *Heterogeneous Photochemical Electron Transfer*; CRC Press: Boca Raton, FL, 1988.

(3) *Photochemical Conversion and Storage of Solar Energy*; Connolly, J. S., Ed.; Academic: New York, 1981.

(4) (a) Fendler, J. H. *Acc. Chem. Res*. **1980**, *13*, 7. (b) Infelta, P. P.; Grätzel, M.; Fendler, J. H. *J. Am. Chem. Soc.* **1980**, *102*, 1479. (c) Dewey, T. G.; Hammes, G. G. *Biophys. J*. **1980**, *32*, 1023. (d) Pileni, M. P. *Chem. Phys. Lett.* **1980**, *71*, 317. (e) Hurst, J. K.; Lee, L. Y. C.; Grätzel, M. *J. Am. Chem. Soc.* **1983**, *105*, 7048.

(5) (a) Kevan, L. In *Photoinduced Electron Transfer, Part B*; Fox, M. A., Chanon, M., Eds.; Elsevier: Amsterdam, 1988; pp 329−384. (b) Kevan, L. *Int. Rev. Phys. Chem*. **1990**, *9*, 307. (c) Kevan, L. *Radiat. Phys. Chem*. **1991**, *37*, 629.

(6) (a) McManus, H. J.; Kang, Y. S.; Kevan, L. *J. Phys. Chem*. **1992**, *96*, 5622. (b) Kang, Y. S.; McManus, H. J.; Kevan, L. *J. Phys. Chem.* **1993**, *97*, 2027. (c) Lanot, M. P.; Kevan, L. *J. Phys. Chem*. **1991**, *95*, 10178. (d) Chastenet de Castaing, E.; Kevan, L. *J. Phys. Chem*. **1991**, *95*, 10178. (e) Kang, Y. S.; Kevan, L. *J. Phys. Chem*. **1994**, *98*, 4389. (f) Sung-Suh, H. M.; Kevan, L. *J. Phys. Chem. A* **1997**, *101*, 1414.

(7) Breck, D. W. *Zeolite Molecular Sieves*; Wiley: New York, 1974.

(8) (a) Persaud, L.; Bard, A. J.; Campion, A.; Fox, M. A.; Mallouk, T. E.; Webber, S. E.; White, J. M. *J. Am. Chem. Soc*. **1987**, *109*, 7309. (b) Kim, Y. I.; Mallouk, T. E. *J. Phys. Chem.* **1992**, *96*, 2879. (c) Yoon, K. B. *Chem. Rev*. **1993**, *93*, 321.

(9) (a) Dutta, P. K.; Incavo, J. A. *J. Phys. Chem.* **1987**, *91*, 4443. (b) Incavo, J. A.; Dutta, P. K. *J. Phys. Chem*. **1987**, *91*, 4443. (c) Borja, M.; Dutta, P. K. *Nature* **1993**, *362*, 43. (d) Ledney, M.; Dutta, P. K. *J. Am. Chem. Soc.* **1995**, *117*, 7687.

(10) Faulkner, L. R.; Suib, S. L.; Renschler, C. L.; Green, J. M.; Bross, P. R. In *Chemistry in Energy Production*; Wymer, R. G., Keller, O. L., Eds.; American Chemical Society: Washington, DC, 1982; pp 99−113.

(11) (a) Stamires, D. N.; Turkevich, J. *J. Am. Chem. Soc.* **1964**, *86*, 749. (b) Dollish, F. R.; Hall, W. K. *J. Phys. Chem.* **1967**, *71*, 1005. (c) Kurita, Y.; Sonoda, T.; Sato, M. *J. Catal.* **1970**, *19*, 82. (d) Slinkin, A. A.; Kucherov, A. V.; Kondrat'ev, D. A.; Bondarenko, T. N.; Rubinshtein, A. M.; Minachev, Kh. M. *J. Mol. Catal.* **1986**, *35*, 97.

(12) (a) Vansant, E. F.; Van Der Voort, P.; Vrancken, K. C. *Characterization and Chemical Modification of the Silica Surface*; Studies in Surface Science and Catalysis, Vol. 93; Elsevier: Amsterdam, 1995. (b) Scott, R. P. W. *Silica Gel and Bonded Phases*; Wiley: Chichester, 1993; Chapters 4 and 6.

(13) (a) Slama-Schwok, A.; Ottolenghi, M.; Avnir, D. *Nature* **1992**, *355*, 240. (b) Slama-Schwok, A.; Avnir, D.; Ottolenghi, M. *J. Am. Chem. Soc.* **1991**, *113*, 3984. (c) Marro, M. A. T.; Thomas, J. K. *J. Photochem. Photobiol. A: Chem.* **1993**, *72*, 251. (d) Bauer, R. K.; Borenstein, R.; De Mayo, P.; Okada, K.; Rafalska, M.; Ware, W. R.; Wu, K. C. *J. Am. Chem. Soc.* **1982**, *104*, 4635. (e) Wilkinson, F.; Worrall, D. R.; Williams, S. L. *J. Phys. Chem*. **1995**, *99*, 6689.

(14) (a) Xiang, B.; Kevan, L. *Colloid Surf. A* **1993**, *72*, 11. (b) Xiang, B.; Kevan, L. *Langmuir* **1994**, *10*, 2688. (c) Matsuura, K.; Kevan, L. *J. Phys. Chem.* **1996**, *100*, 10652.

(15) (a) Wasielewski, M. R. *Chem. Rev*. **1991**, *92*, 435. (b) Fajer, J.; Davis, M. In *The Porphyrins*; Dolphin, D., Ed.; Academic: New York, 1979; Vol. 4, Chapter 4. (c) Fajer, J.; Borg, D. C.; Forman, A.; Felton, L. V.; Dolphin, D. *Ann. N.Y. Acad. Sci*. **1973**, *206*, 349. (d) Felton, R. H. In *The Porphyrins*; Dolphin, D., Ed.; Academic: New York, 1979; Vol. 5, Chapter 2.

(16) (a) Gouterman, M. In *The Porphyrins*; Dolphin, D., Ed.; Academic: New York, 1978; Vol. 2, Chapter 1. (b) Burgess, R. M.; Gouterman, M.; Khail, G.-E.; Van Zee, J. In *Porphyrins: Excited States and Dynamics*; Gouterman, M., Ed.; American Chemical Society: Washington, DC, 1986; ACS Symposium Series No. 321, pp 328−346. (c) Gouterman, M.; Khalil, G.-E. *J. Mol. Spectrosc.* **1974** *53*, 88.

(17) (a) Harriman, A.; Porter, G.; Richoux, M. C. *J. Chem. Soc., Faraday Trans. 2* **1981**, *77*, 1175. (b) Rotenberg, M.; Margalit, R. *Biochem. Biophys. Acta* **1987**, *905*, 173. (c) Groves, J. T.; Newman, R. *J. Am. Chem. Soc*. **1989**, *111*, 2900. (d) Kalyanasundaram, K.; Vlachopoulos, N.; Krishnan, V.; Monnier, A.; Grätzel, M. *J. Phys. Chem*. **1987**, *91*, 2342.

(18) Hamor, M. J.; Hamor, T. A.; Horad, J. L. *J. Am. Chem. Soc.* **1964**, *86*, 1938.

(19) (a) Kresge, C. T.; Leonowicz, M. E.; Roth, W. J.; Vartuli, J. C.; Beck, J. S. *Nature* **1992**, *359*, 710. (b) Beck, J. S.; Vartuli, J. C.; Roth, W. J.; Leonowicz, M. E.; Kresge, C. T.; Schmitt, K. D.; Chu, C. T.-W.; Olson, D. H.; Sheppard, E. W.; McCullen, B.; Higgins, J. B.; Schlenker, J. L. *J. Am. Chem. Soc*. **1992**, *114*, 10834. (c) Beck, J. S.; Vartuli, J. C.; Kennedy, G. J.; Kresge, C. T.; Roth, W. J.; Schramm, S. E. *Chem. Mater*. **1994**, *6*, 1816. (d) Vartuli, J. C.; Schmitt, K.; Kresge, C. T.; Roth, W. J.; Leonowicz, M. E.; McCullen, B.; Hellring, S. D.; Beck, J. S.; Schlenker, J. L.; Olson, D. H; Sheppard, E. W. In *Zeolites and Related Microporous Materials: State of the Art 1994*; Weitkamp, J., Karge, H. G., Pfeifer, H., Holderich, W., Eds.; Studies in Surface Science and Catalysis, Vol. 84; Elsevier: Amsterdam, 1994; pp 53−60.

(20) Stucky, G. D.; Monnier, A.; Schuth, F.; Hou, Q.; Margolese, D.; Kumar, D.; Kridhnamurty, M.; Petroff, P.; Firouzi, A.; Janicke, M.; Chmelka, B. F. *Mol. Cryst. Liq. Cryst.* **1994**, *240*, 187.

(21) (a) Luan, Z.; Cheng, C.-F.; Zhou, W.; Klinowski, J. *J. Phys. Chem*. **1995**, *99*, 1018. (b) Alba, M. D.; Luan, Z.; Klinowski, J. *J. Phys. Chem*. **1996**, *100*, 2179. (c) Cheng, C.-F.; He, H.; Zhou, W.; Klinowski, J.; Goncalves, J. A. S.; Gladden, L. F. *J. Phys. Chem*. **1996**, *100*, 390.

(22) (a) Zhao, D.; Goldfarb, D. *J. Chem. Soc., Chem. Commun*. **1995**, 875. (b) Reddy, K. M.; Moudrakovski, I.; Sayari, A. *J. Chem. Soc., Chem. Commun*. **1994**, 1059.

(23) (a) Corma, A.; Navarro, M. T.; Pérez-Pariente, J.; Sanchez, F. In *Zeolites and Related Microporous Materials: State of the Art 1994*; Weitkamp, J., Karge, H. G., Pfeifer, H., Holderich, W., Eds.; Studies in Surface Science and Catalysis, Vol. 84; Elsevier: Amsterdam, 1994; pp 69−75. (b) Tuel, A. *Zeolites* **1995**, *15*, 228. (c) Franke, O.; Rathousky, J.; Ekloff, G. S.; Starek, J. In *Zeolites and Related Microporous Materials: State of the Art 1994*; Weitkamp, J., Karge, H. G., Pfeifer, H., Holderich, W., Eds.; Studies in Surface Science and Catalysis, Vol. 84; Elsevier: Amsterdam, 1994; pp 77−89. (d) Thomas, J. M.; Greaves, G. N. *Science* **1994**, *265*, 1675. (e) Maschmeyer, T.; Rey, F.; Sankar, G.; Thomas, J. M. *Nature* **1995**, *378*, 159.

(24) (a) Notari, B. *Adv. Catal*. **1996**, *41*, 258. (b) Blasco, T.; Corma, A.; Navaro, M. T.; Pere-Pariente, J. *J. Catal*. **1995**, *156*, 65. (c) Anpo, M.; Nakaya, H.; Kodama, S.; Kubokawa, Y. *J. Phys. Chem.* **1986**, *90*, 1633. (d) Liu, Z.; Davis, R. J. *J. Phys. Chem.* **1994**, *98*, 1253. (e) De Castro-Martins, S.; Tuel, A.; Ben Taarit, Y. *Zeolites* **1994**, *14*, 130.

(25) (a) Corma, A.; Fornes, V.; Garcia, H.; Miranda, M. A.; Sabater, A. *J. Am. Chem. Soc*. **1994**, *116*, 9767. (b) Cano, M. L.; Cozens, F. L.; Garcia, H.; Marti, V.; Scaiano, J. C. *J. Phys. Chem.* **1996**, *100*, 18152.

(26) Cullity, B. D. *Elements of X-ray Diffraction*; Addison-Wesley: Reading, MA, 1987; p 87.

(27) Feuston, B. P.; Higgins, J. B. *J. Phys. Chem.* **1994**, *98*, 4459.

(28) Ravikovitch, P. I.; Wei, D.; Chueh, W. T.; Haller, G. L.; Neimark, A. V. *J. Phys. Chem. B* **1997**, *101*, 3671.

(29) (a) Offen, H. W. In *Organic Molecular Photophysics*; Birks, J. B., Ed.; Wiley: London, 1973; Vol. 1, Chapter 3. (b) Lesclaux, R.; Joussot-Dubien, J. In *Organic Molecular Photophysics*; Birks, J. B., Ed.; Wiley: London, 1973; Vol. 1, Chapter 9.

(30) (a) Harriman, A. *J. Chem. Soc., Faraday Trans. 1* **1980**, *76*, 1978. (b) Darwent, J. R.; Douglas, P.; Harriman, A.; Porter, G.; Ricjoux, M.-C. *Coord. Chem. Rev* **1982**, *44*, 83.

(31) (a) Leermkers, P. A.; Thomas, H. T.; Weis, L. D.; James, F. C. *J. Am. Chem. Soc*. **1966**, *88*, 5075. (b) Ron, A.; Folman, M.; Schnepp, O. *J. Phys. Chem*. **1962**, *36*, 2449.

(32) (a) Mochida, I.; Tsuji, K.; Suetsugu, K.; Fujitsu, H.; Takeshida, K. *J. Am. Chem. Soc.* **1980**, *84*, 3159. (b) Lexa, D.; Reix, M. *J. Chim. Phys.* **1974**, *71*, 24. (c) Stone, A.; Fleischer, E. B. *J. Am. Chem. Soc.* **1968**, *90*, 2735.

(33) Pimentel, G. C.; Spratley, R. D. *Chemical Bonding Clarified through Quantum Mechanics*; Holden-Day: San Francisco, 1969; Chapter 8.

(34) (a) Di Renzo, F.; Chiche, B.; Fajula, F.; Viale, S.; Garrone, E. In *11th International Congress on Catalysis-40th Anniversary*; Hightower, J. W., Delgass, W. N., Iglesia, E., Eds.; Studies in Surface Science and Catalysis, Vol. 101; Elsevier: Amsterdam, 1996; pp 851−860. (b) Le Noc, L.; Trong On, D.; Solomykina, S.; Echchahed, B.; Béland, F.; Cartirt dit Moulin, C.; Bonneviot, L. In *11th International Congress on Catalysis−40th Anniversary*; Hightower, J. W., Delgass, W. N., Iglesia, E., Eds.; Studies in Surface Science and Catalysis, Vol. 101; Elsevier: Amsterdam, 1996; pp 611−620.

(35) (a) Brus, L. E. *J. Chem. Phys.* **1984**, *80*, 4403. (b) Kubo, R.; Kawabata, A.; Kabayashi, S. *Annu. Rev. Mater. Sci.* **1984**, *14*, 49. (c) Wang, Y.; Suna, A.; Mahler, W.; Kasowski, R. *J. Chem. Phys.* **1987**, *87*, 7315.

(36) (a) Deo, G.; Wachs, I. E. *J. Catal.* **1991**, *129*, 307. (b) Topsoe, N.-Y. *Science* **1994**, *265*, 1217.

(37) (a) Taramaso, M.; Perego, G.; Notari, B. U.S. Patent 4 410 501, 1983. (b) Tuel, A.; Ben Taarit, Y. *Appl. Catal. A* **1993**, *102*, 69. (c) Blasco, T.; Camblor, M. A.; Corma, A.; Perez-Pariente, J. *J. Am. Chem. Soc.* **1993**, *115*, 11806.

(38) Luan, Z.; Kevan, L. *J. Phys. Chem. B* **1997**, *101*, 2020.

(39) Tuel, A.; Diab, J.; Gelin, P.; Dufaux, M.; Dutel, J.-F.; Ben Taarit, Y. *J. Mol. Catal.* **1991**, *68*, 45.

(40) Huybrechts, D. R. C.; Buskens, P. L.; Jacobs, P. A. *J. Mol. Catal.* **1985**, *31*, 355.